Journal of Power Sources 270 (2014) 166–182

Contents lists available at ScienceDirect

Journal of Power Sources

journal homepage: www.elsevier.com/locate/jpowsour

Effectiveness of heat-integrated methanol steam reformer and polymer electrolyte membrane fuel cell stack systems for portable applications

A. Lotrič [a, b], M. Sekavčnik [b, *], S. Hočevar [a, c]

[a] Mebius d.o.o., Na Jami 3, SI-1000 Ljubljana, Slovenia
[b] University of Ljubljana, Faculty of Mechanical Engineering, Aškerčeva 6, SI-1000 Ljubljana, Slovenia
[c] National Institute of Chemistry Slovenia, Hajdrihova 19, SI-1000 Ljubljana, Slovenia

HIGHLIGHTS

- A concept of compact, heat integrated system of PEMFC stack and methanol steam reformer (MSR) is proposed.
- Three separate systems are designed based on different types of PEMFC stacks.
- Proposed novel HT PEMFC (nHT PEMFC) stack operates at 255 °C which matches the MSR operating at 250 °C.
- Systems are compared using mass and energy balances model coupled to a physical model.
- Highest efficiency is attained by the system with nHT PEMFC stack operating at 255 °C.

ARTICLE INFO

Article history:
Received 12 May 2014
Received in revised form
2 July 2014
Accepted 11 July 2014
Available online 21 July 2014

Keywords:
Fuel processor
PEM fuel cell
Methanol steam reformer
Heat integrated system

ABSTRACT

Efficiently combining proton exchange membrane fuel cell (PEMFC) stack with methanol steam reformer (MSR) into a small portable system is still quite a topical issue. Using methanol as a fuel in PEMFC stack includes a series of chemical processes where each proceeds at a unique temperature. In a combined MSR–PEMFC-stack system with integrated auxiliary fuel processors (vaporizer, catalytic combustor, etc.) the processes are both endothermic and exothermic hence their proper thermal integration can help raising the system efficiency. A concept of such fully integrated and compact system is proposed in this study. Three separate systems are designed based on different PEMFC stacks and MSR. Low-temperature (LT) and conventional high-temperature (cHT) PEMFC stack characteristics are based on available data from suppliers. Also, a novel high-temperature (nHT) PEMFC stack is proposed because its operating temperature coincides with that of MSR. A comparative study of modelled systems is performed using a mass and energy balances zero-dimensional model, which is interdependently coupled to a physical model based on finite element method (FEM). The results indicate that a system with nHT PEMFC stack is feasible and has the potential to reach higher system efficiencies than systems with LT or cHT PEMFC stacks.

1. Introduction

Although PEMFC technology is already quite mature a number of key obstacles still remain for their successful realization as a high-energy density standalone portable or stationary power sources. One of the major constraints for the PEMFCs is that they use hydrogen as a fuel which has a very low energy density per volume at conditions of standard ambient temperature and pressure (SATP). Therefore, pure hydrogen is stored either as gas at very high pressures (up to 800 bar) or as liquid at very low temperatures below −253 °C. Hydrogen is not a naturally occurring energy source on Earth; it is actually just an energy carrier and it has to be produced from other sources using various processes (e.g. electrolysis, gasification or reforming). As energy carrier methanol is also showing promise because at SATP, compared to hydrogen at 800 bar, it still has more than 2.6 times higher energy density per volume and is in liquid form which greatly facilitates its storage and transportation.

* Corresponding author. Tel.: +386 1 4771 303.
E-mail address: mihael.sekavcnik@fs.uni-lj.si (M. Sekavčnik).

http://dx.doi.org/10.1016/j.jpowsour.2014.07.072
0378-7753/

Methanol as a fuel can be used in PEMFC directly in a so-called direct methanol fuel cell (DMFC) or it can be transformed into hydrogen rich gas using an on-site reformer. Although systems using DMFCs are simpler comparing to combined systems with methanol reformer and PEMFCs, far greater energy densities are archived with combined systems. Methanol steam reforming is more attractive than methanol auto-thermal reforming because of its higher attainable hydrogen concentration and smaller amount of carbon monoxide (CO) in the reformate stream. Unfortunately even a small amount of CO in the incoming stream presents a severe limitation for LT PEMFC. At operating temperatures around 80 °C CO tends to strongly adsorb onto the active sites of platinum (Pt) and thus poisons the catalyst. Cleaning processes like water-gas shift (WGS) and/or preferential oxidation (PROX) are needed to reduce the concentration of CO. Typical operating temperatures for PROX are somewhere between 100 and 200 °C although sometimes they are even outside this range [1]. There are several approaches to overcoming the CO poisoning of electrocatalysts [2]. With Pt–Ru catalyst around 10 ppm of CO can be tolerated in the stream [3] or with air-bleeding technique even up to 200 ppm [4].

The phenomenon of CO adsorption on Pt is far less pronounced at higher temperatures [5]. That is why cHT PEMFC based on polybenzimidazole (PBI) polymer doped with phosphoric acid (H_3PO_4) can still operate reasonably unaffected at temperatures above 160 °C and can tolerate up to several percent of CO in hydrogen rich gas stream. Several studies have confirmed that [6–8]; also datasheets from commercial suppliers are available [9,10]. Other advantages of cHT PEMFCs over LT PEMFCs are simplified water management because no humidification is necessary and during operation only water vapour is present in the system which eliminates the possibility of flooding the cathode channels. Heat is produced at a higher temperature level and can be used to preheat gases, vaporise water–methanol mixture or to produce hot water and/or steam in industrial or home applications.

Despite higher tolerance of cHT PEMFC to CO a major drawback is the adsorption of acid anions ($H_2PO_4^-$) on the active sites of the Pt catalyst [11]. In spite of higher temperatures this slows down the oxygen reduction reaction (ORR) kinetics more than in the case of LT PEMFC, hence, lower power density is achieved. Phosphoric acid is also highly soluble in water and can leach out from the membrane especially if the fuel cell is exposed to frequent start–stop cycles because liquid water can be present in the system. Its vapour pressure is highly temperature and concentration dependent [12] (e.g. at atmospheric pressure an 85% concentrated H_3PO_4 starts boiling at 158 °C while 100% concentrated H3PO4 at 261 °C). The lower temperature limit of cHT PEMFC is about 130 °C at which temperature water is in vapour phase. At temperatures higher than 155 °C an equilibrium is established between orthophosphoric acid and highly water-soluble pyrophosphoric acid:

$$2H_3PO_4 \leftrightarrow H_4P_2O_7 + H_2O \quad (1)$$

At higher temperatures further condensation of phosphoric acid leads to polyphosphoric acid. Steady decline in conductivity at long-term operation of H_3PO_4/PBI membranes is explained in terms of influence of water concentration (activity) formed on cathode side, which leads to the hydrolysis of polyphosphoric acid and leaches out water-soluble orthophosphoric and pyrophosphoric acids. On the other side, at temperatures higher than 180 °C, the vapour pressure of phosphoric acid becomes prohibitively high, which again leads to losses of acid from the fuel cell [13].

The main challenge of every energy system is to recuperate heat available within the system to maximize its efficiency. Since some unit reactions in combined PEMFC systems are exothermic (catalytic combustion, PROX) and others endothermic (vaporisation, MSR) the goal is to direct the heat from sources to sinks within the system (see also Fig. 1). The most obvious step that applies such action is the direct thermal coupling of the MSR and the HT PEMFC stack which can be done in two ways. One is to use existing, cHT PEMFCs and develop a new catalyst that would allow the MSR to operate at temperatures below 200 °C and still achieve near to 100% conversion rate of methanol. First results on development of LT MSR have already been published by a research group claiming to achieve 100% conversion at 195 °C [14,15]. The second way is the use of conventional catalyst in the MSR which enables to attain practically full conversion of methanol between 250 °C–300 °C. This however depends on the geometry, flow characteristics, catalysts loading, and steam-to-carbon ratio (S/C). Typically, conversions above 95% are achieved at 250 °C with $S/C \leq 2{:}1$ [16–20] while some researches also achieved 100% conversion with $S/C \leq 1.5{:}1$ [21,22]. Since all conventional PEMFCs operate at lower temperature as the MSR there is a need for development of nHT PEMFC that could operate at temperatures higher than 250 °C and consequently enable direct thermal coupling of the nHT PEMFC stack and the MSR. Some research efforts in this direction have been published recently with development of so-called solid acid fuel cell (SAFC) [23,24] although first publications on this topic date back several years ago [25–27].

There are researches devoted to thermal coupling of the catalytic combustor and the MSR [17,19,20,22]. One research even tried coupling the stack of cHT PEMFCs and the MSR [21]. Some studies on the integrated systems where all of fuel processing reactors are combined together in the system are available. There are numerical studies of such systems but they are more focused on the implementation [28] and dynamics [29,30] of the whole system. A related numerical study [31] on stationary integrated system for a small household with glycerol reforming process and PEMFC stack showed that a system with LT PEMFC stack has lower electric efficiency than the system with cHT PEMFC stack when a WGS process is used in both cases. If heat generated in the PEMFC stack is used to produce hot water at 50 °C for household usage the combined efficiencies of both systems are increased to 60%. More in-depth insight to the design of small compact systems was presented in Ref. [32] although the PEMFC stack was excluded from the analysis. Beside numerical calculations also an experimental system was constructed by the same authors in their previous work [33]. Concept and experimental data of compact, highly integrated system was presented in Refs. [34,35] although in experiments the stack of cHT PEMFCs was not thermally coupled to the fuel processing units. Another research group published the experimental

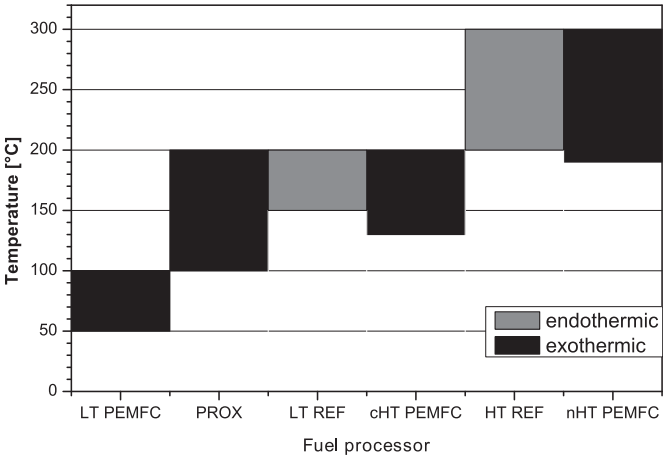

Fig. 1. Fuel processors sorted according to their operating temperature range.

results of the fully integrated system although the method of integration is not explained in detail due to confidentiality reasons [18,36].

As it is explained in Ref. [32] a proportionately higher rate of heat loss occurs as size of the object is reduced. Hence, it is essential to control heat losses if energy efficiency is to be attained. In a small system fuel processing reactors are necessarily extremely proximate, and yet must be allowed to attain unique temperatures that are optimal for their operation. Because elements in thermal contact tend to approach the same temperature a strategy for thermal insulation of individual fuel processors and the system as a whole is a necessity.

The main objective of this paper is to study and compare the heat-integrated systems capable of producing 25 W of gross electric power for use in portable applications. All fuel processing reactors (including fuel cells) have planar configuration and are stacked into a compact form. For this purpose we analyse three possible system configurations:

a) A system with microreactor based MSR operating between 230 and 250 °C combined with LT PEMFC;
b) A system with microreactor based MSR operating between 230 and 250 °C combined with cHT PEMFC (PBI derived membranes doped with phosphoric acid) that operate between 130 and 200 °C;
c) A system with microreactor based MSR operating between 230 and 250 °C combined with nHT PEMFC that operate between 190 and 300 °C.

2. Description of integrated MSR–PEMFC-stack systems

The objective of this study is not to design in detail the integrated systems because even though the conceived systems are small and compact they still require certain Balance-of-Plant (BoP) components for their operation (e.g. sensors, actuators, control systems, blowers and/or pumps etc.). Therefore, BoP components are neglected from this study despite the fact that they can have a significant impact on the system efficiency. Also, design and optimization of system components such as shape and size of fluid flow channels within fuel processors is not the focus of this study. The goal is to quantitatively assess the energy flows within the proposed systems based on heat production/consumption and heat transfer between the system components.

Three different cases of integrated systems are conceived and compared between each other. They are designed in such a way that they achieve 25 W of (gross) electric power at their nominal operating conditions. The same principle is used to design all the systems; however, different operating temperatures of the PEMFC stacks dictate different internal arrangements of components. All the systems are built from planar-type components (e.g. end plates, bipolar plates, fuel processors) where their base surface area always measures 7 × 7 cm^2 but their thicknesses varies. The system components are stacked together into a compact form and arranged in a thermal cascade where the hottest heat source (catalytic combustor) is placed in the middle of the system while the rest of heat sources and sinks are arranged according to their operating temperatures. The integration of catalytic combustor also enables heating-up the system to the required temperatures at start-up. In addition, hot air can be blown through the cathode side of the PEMFC stack as shown in Refs. [37,38]. Clamping of the system, input and output connectors, gaskets and electric terminals are not taken into consideration in the study. However, it is presumed that the active surface area or in other words the PEMFC electrodes measure 5 × 5 cm^2. This leaves a rectangular stripe 1 cm wide, measuring from the sides towards the centre of all system components, which can be applied for sealing and allocation of main fluid channels. All the processes are assumed to proceed at ambient pressure $p_{AMB} = 1$ bar without any pressure losses.

It is considered that water and methanol reside in two separate containers and are mixed prior to entering the vaporiser. Part of the water in the system can be recycled although looking from stoichiometric point of view the production vs. consumption ratio of water in the system is 3:1.

Consumption of water in MSR:

$$H_2O + CH_3OH \rightarrow CO_2 + 3H_2 \quad (2)$$

Production of water in PEMFC:

$$3H_2 + 1.5O_2 \rightarrow 3H_2O \quad (3)$$

In a real system this ratio will be lower because above stoichiometric ratio of water is used in MSR, also not all of methanol is successfully converted, and hydrogen utilization in PEMFC is not 100%. Nonetheless, water in the system will still be in surplus therefore the water container needs to be properly sized to store all the produced water. Issues involving water management in the system are not taken into account in the present study but they will need to be considered in the following studies.

For the quantitative assessment of heat utilisation and comparison between the three systems it is assumed that the heat carried by the flue gases leaving the system is recuperated in some other (external) process which consequently cools down the stream to 40 °C. A convenient way to do this could be the use of thermo electric generators (TEG) as proposed in Ref. [39]. This way some additional electric power can be produced and used to power the BoP components. To assess the heat flow rejected to the surroundings and to close the energy balance of the system the exiting stream is further cooled down to the temperature of surroundings $T_{SURR} = 20$ °C.

All the systems are air cooled via forced convection which means that air is supplied to the system in over stoichiometric ratio in order to keep the PEMFC stack operating at desired, isothermal conditions. As shown in Ref. [40] it is reasonable to assume that air enters from the side of the PEMFC stack through an open-cathode where air is supplied by a blower. Selection of appropriate air blower or design of cathode distribution channels within the stack is not the focus of this research, the same holds for methanol pump and anode distribution channels. On exit air is collected in a channel and routed around the system according to the flowcharts given in subsequent subsections.

To establish and maintain the required temperatures of individual fuel processors a special insulating material needs to be used around and also within the system. This material must have extremely good insulating properties and concurrently good compression resistance because the fuel processors need to be pressed together with adequate stress to enable good contact for heat transfer and to reduce ohmic resistance between PEMFCs. With advances in material technologies the above mentioned criteria are met by modifying the conventional Aerogel material. Cross-linking the Aerogel polymer structure enables the new material (X-Aerogel) to retain extremely good insulating properties of its predecessor but at the same time to be much more resistant to compression stresses [41].

The systems are presented in cross-sectional views and in form of schematic flowcharts where fuel processor temperatures are given in square brackets and stream temperatures without square

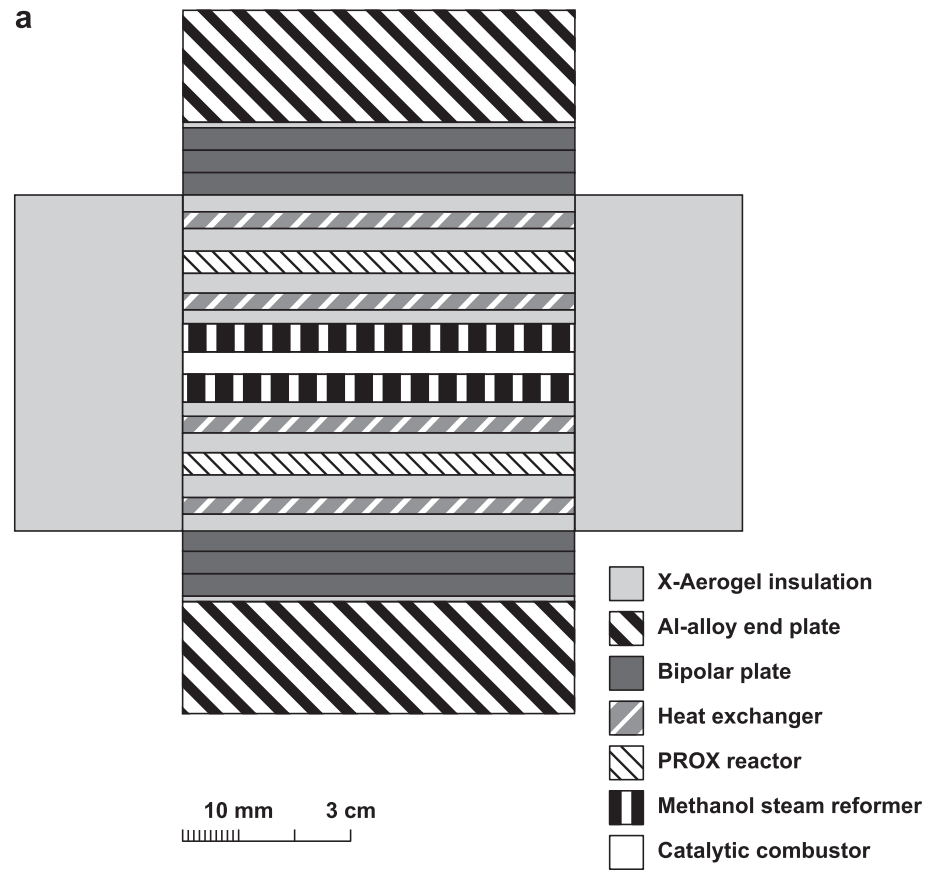

Fig. 2. Integrated system with LT PEMFC stack: (a) cross sectional view, (b) flowchart diagram.

brackets. Also, produced or consumed heat flows of individual fuel processors are given.

2.1. Integrated system with LT PEMFC stack

The integrated system with LT PEMFC stack comprises of catalytic combustor, MSR, PROX reactor, heat exchangers, Al-alloy end plates and insulation as shown in Fig. 2(a). The insulation around the system prevents extensive heat losses from the fuel processors with exception of the LT PEMFC stack which is uninsulated and allowed to also cool by natural convection. The inner insulating layers are used to establish and maintain the required temperatures within the system. The first heat exchanger, located between the LT PEMFC stack and the PROX reactor, is also a vaporiser for the

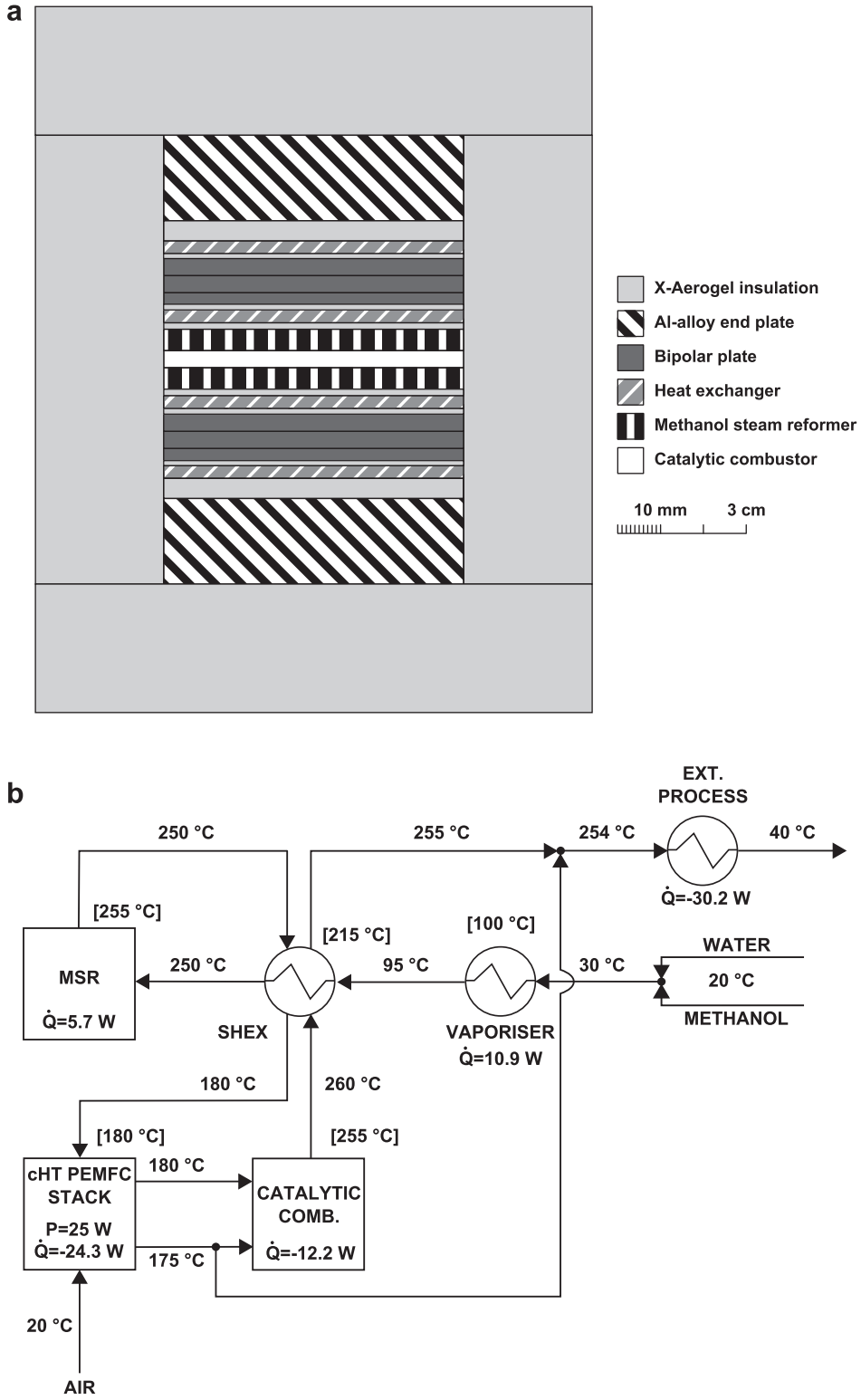

Fig. 3. Integrated system with cHT PEMFC stack: (a) cross sectional view, (b) flowchart diagram.

water–methanol mixture. Here, the flue gases and the reformate stream exiting the PROX reactor are cooled down and transfer the heat to the water–methanol mixture which is evaporated and then slightly superheated. In the second heat exchanger, located between the PROX reactor and the MSR, heat transferred from the flue gases and the reformate stream superheats the water–methanol mixture up to 250 °C before entering the MSR. The exit stream form the MSR enters first the PROX reactor. The heat released during the PROX reaction helps to retain the thermal cascade within the system. After reducing the CO concentration to less than 10 ppm the stream exiting the PROX reactor is cooled down to 70 °C and routed into the LT PEMFC stack. Air is supplied to the LT PEMFC stack with over stoichiometric ratio; therefore, there is still considerable amount of oxygen left in the cathode off-gas stream. Part of this stream is routed in the PROX reactor, part of it in the catalytic combustor while part of it bypasses the combustor and recombines with exiting flue gases (see Fig. 2(b)). Bypass is used with the aim of reducing the methanol consumption because less mass needs to be heated to the operating temperature of combustor. The catalytic combustor requires additional methanol because the anode off-gas stream itself cannot produce enough heat to fully vaporise the water–methanol mixture and to keep the MSR operating at 250 °C.

2.2. Integrated system with conventional HT PEMFC stack

The integrated system with cHT PEMFC stack comprises of catalytic combustor, MSR, heat exchangers, Al-alloy end plates and insulation as shown in Fig. 3(a). The system is entirely insulated to prevent extensive heat losses from the cHT PEMFC stack operating at 180 °C and from other fuel processors. Inner insulating layers are again used to establish and maintain the required temperatures

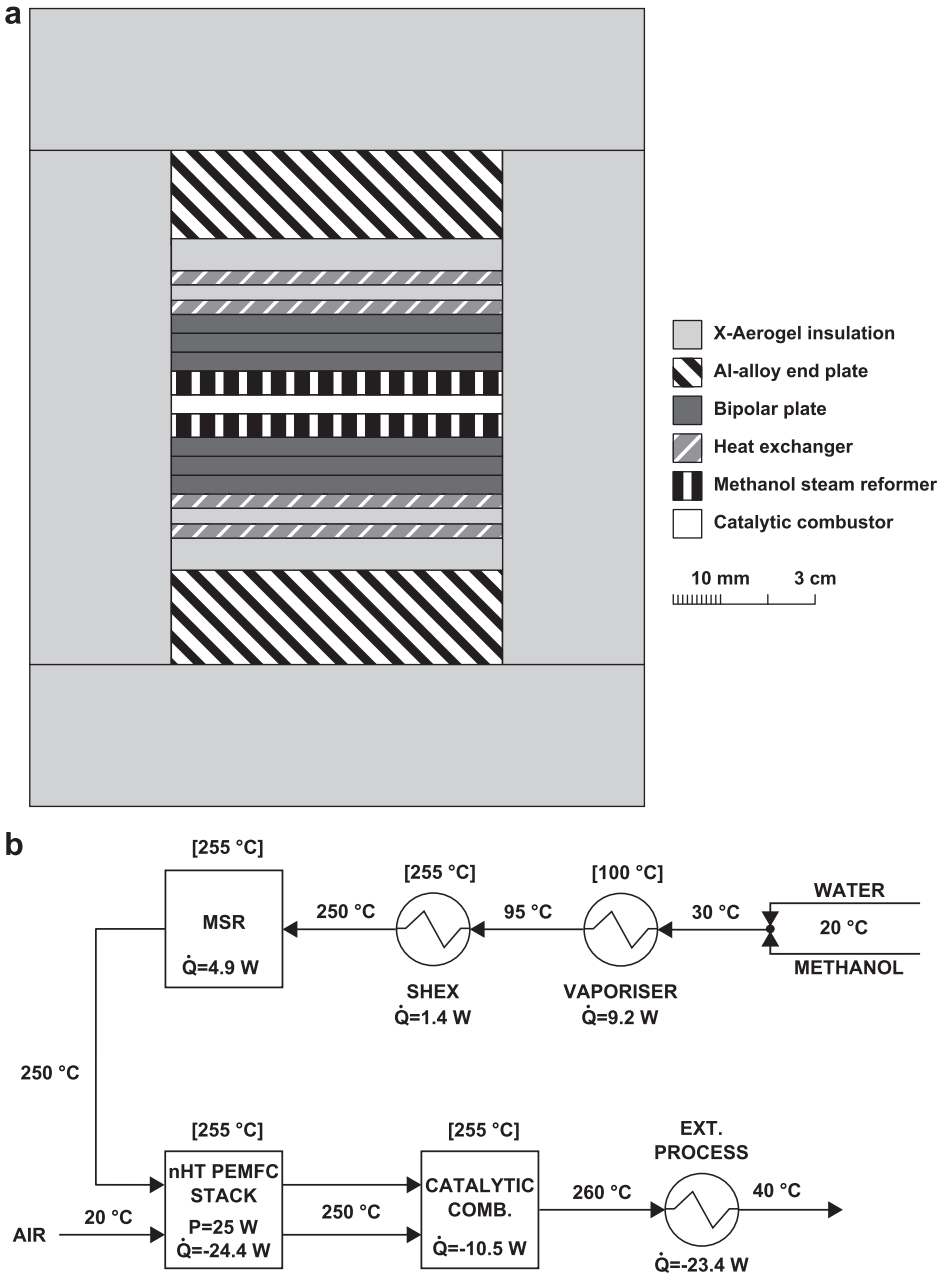

Fig. 4. Integrated system with nHT PEMFC stack: (a) cross sectional view, (b) flowchart diagram.

within the system. Even though the heat produced in the stack is not on sufficiently high temperature level to supply heat to the MSR, this heat is well suited for use in the first heat exchanger which vaporises and slightly superheats the water–methanol mixture. In the second heat exchanger, located between the cHT EPMFC stack and the MSR, the flue gases and the reformate stream are cooled down and the water–methanol mixture is preheated to 250 °C before entering the MSR. Stream exiting the MSR needs no CO clean-up and is directly led to the cHT PEMFC stack. The anode off-gas from cHT PEMFC stack still possesses enough calorific value that no additional methanol is needed for the catalytic combustor to produce heat for the MSR. For cooling purposes air is supplied to the cHT EPMFC stack with over stoichiometric ratio. Part of the cathode off-gas stream is led to the catalytic combustor while part of it bypasses the combustor and recombines with flue gases. Here, the purpose of bypass is to allow the flue gases exiting the combustor to attain 260 °C. The flowchart of the system is presented on Fig. 3(b).

2.3. Integrated system with novel HT PEMFC stack

The integrated system with nHT PEMFC stack comprises of catalytic combustor, MSR, heat exchangers, Al-alloy end plates and insulation as shown in Fig. 4(a). The system is entirely insulated to prevent extensive heat losses because of the high operating temperatures of the fuel processors. Only the vaporiser for the water–methanol mixture operates at lower temperature and is insulated from both sides to attain the required temperature. The nHT PEMFC stack operates at 255 °C and supplies heat to the MSR and the superheater through direct contact. In this case there is actually no need for the catalytic combustor and the anode off-gas stream could also be recycled within the system. However to simplify the system, the anode off-gas is still burned in the catalytic combustor and the produced heat is used to partly compensate for heat losses while some of it is extracted from the flue gases and used as heat in the external energy process. Over stoichiometric ratio of air again allows to regulate the operating temperature of the nHT PEMFC stack and to later use the off-gas stream to supply oxygen to the catalytic combustor. The flowchart of the system is presented on Fig. 4(b).

As mentioned in introduction first steps towards nHT PEMFC have already been taken. However, there are certain disadvantages that the SAFC possess. At ambient pressure it operates in a relatively narrow temperature region. Around 230 °C the polymorphic, structural transition in solid acid electrolyte occurs and the protonic conductivity is raised by several orders of magnitude (superprotonic state). The electrolyte is stabile only if dehydration is prevented which means that at 230 °C it needs to be exposed to humidified atmosphere containing slightly less than 10% of water while at 280 °C 40% of water is needed [27]. In the superprotonic state also high plasticity emerges which causes certain durability issues. Nevertheless, relatively high peak power densities have been achieved where some are even comparable to those of cHT PEMFCs with 415 mW cm^{-2} [26]. The results exceeding cHT PEMFC were presented in Ref. [27] with more than 600 mW cm^{-2} under normal conditions of 80% and 50% hydrogen and air utilization, respectively. However, the results were achieved by replacing the Pt cathode catalyst with a $Pt_{0.2}Pd_{0.8}$ alloy. Also, tolerance to CO levels as high as 20% in hydrogen rich gas has been demonstrated.

In this study it is considered that a novel nanocomposite polymer membrane with a water-insoluble solid proton conducting electrolyte is used. This eliminates problems of SAFC (water management of electrolyte) and cHT PEMFC (e.g. H_3PO_4 leaching, adsorption of $H_2PO_4^-$, etc.) and allows reaching temperatures up to 300 °C which for modern polymers (e.g. PBI or polyimide) presents no major problems. At this point it is fair to mention that no such commercial nHT PEMFC exists, although, the technology and materials to build such an assembly are already at hand. However, there are several issues that need to be resolved prior to constructing such systems. Firstly, a new solid electrolyte that is capable to provide sufficient proton conductivity without the presence of water needs to be developed. Secondly, high temperatures present a major problem for gasket materials; therefore, care needs to be taken when selecting the appropriate material. It is extremely difficult for conventional rubber or Teflon based gaskets to withstand long-term exposures to temperatures above 250 °C with an exception of Kalrez® which is extremely expensive. Generally, high temperatures also reduce the resistance of gaskets to compression set which reduces effective sealing force and can result in leakage. Thirdly, corrosion of carbon support for Pt catalyst is accelerated at high temperatures. This phenomena is well known to already occur at operating temperatures of cHT PEMFC [42]. Therefore, it is expected that a new support for the Pt catalyst will need to be developed for the nHT PEMFC.

3. Simulation approach

Two different pathways are used to more thoroughly examine the conceived systems. First, applies a zero-dimensional model based on mass and energy balances of the systems. This is done by using Aspen Plus® simulation software where all the system model units are studied at their operating, isothermal and stationary conditions. Second, uses COMSOL Multiphysics® software to simulate physical models of integrated systems. Here, heat transfer is also studied at stationary conditions where the volume average temperature of model units closely corresponds to the temperatures used in mass and energy balance calculations. The two pathways are interdependent and coupled together as shown in Fig. 5.

3.1. Calculation process

The initial values for a zero-dimensional model are the temperatures of individual processes $T_{PROCESSES}$, the methanol molar flow $\dot{n}_{MeOH,\,IN}$, and the molar flow of cathode air which is expressed in terms of excess air ratio $\lambda_{AIR,\,IN}$ and is prescribed by commercial suppliers of PEMFCs. The initial values for a physical model are the dimensions (geometry) of system components where the base surface area always measures 7 × 7 cm^2 but the thicknesses of components vary and are given in Table 3. The initial thicknesses of inner insulating layers $d_{INSU,IN}$ also need to be given and are estimated by means of first approximation methods.

First, mass and energy balances of the systems are calculated using the zero-dimensional model. The sensitivity analysis of methanol molar flow at prescribed excess air ratios is performed for each system. The operation point where 25 W of electric power is reached determines the nominal molar flow of methanol. Once the operation point is set it does not change anymore because it is presumed that changing the molar flow of methanol dictates the PEMFC stack power output. Increasing excess air ratio due to air cooling will at most help to raise the power output of the PEMFC stack because more oxygen can establish the three-phase boundary layer inside the PEMFC where the ORR takes place.

In the next step the iterative trial-and-error process is executed. Information on calculated heat flows in the system model units are inserted into physical model of the compact, integrated system where heat transfer among individual components is studied. The iterative process is stopped when the values of certain parameters match in both models. These parameters are the heat removed by air cooling $\dot{Q}_{AIR}$ and the temperatures of individual processes. If

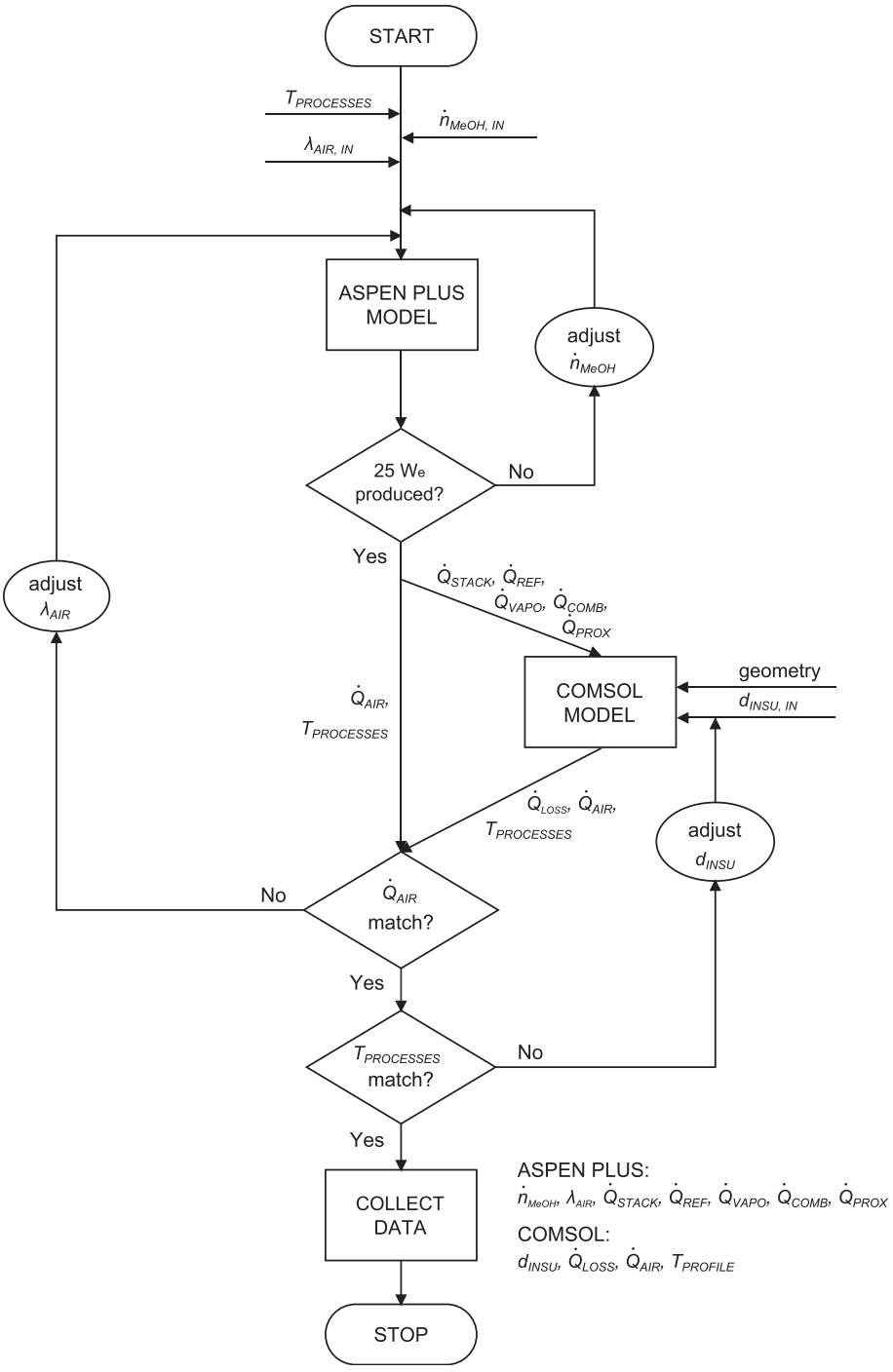

Fig. 5. Simulation algorithm.

these conditions are not met the excess air ratio λ_{AIR} and the thicknesses of inner insulating layers d_{INSU} are varied until the conditions are fulfilled. When the iterative process ends all data are collected (see also Fig. 5). From mass and energy balances calculations in Aspen Plus® the following data are obtained: methanol flow to produce 25 We $\dot{n}_{MeOH}$, excess air ratio λ_{AIR}, heat flow produced by the PEMFC stack $\dot{Q}_{STACK}$, heat flow consumed by the MSR $\dot{Q}_{REF}$, heat flow needed to vaporise water–methanol mixture $\dot{Q}_{VAPO}$, heat flow produced by the combustor $\dot{Q}_{COMB}$, and in case of LT PEMFC stack also the heat flow produced by the PROX reactor $\dot{Q}_{PROX}$. Data obtained from the physical modelling of the systems in COMSOL Multiphysics® are thicknesses of inner insulating layers d_{INSU}, heat losses of the integrated system $\dot{Q}_{LOSS}$, heat flow removed from the PEMFC stack with cooling air $\dot{Q}_{AIR}$, and the temperature profile of the designed system $T_{PROFILE}$.

3.2. Adopted simplifications in heat transfer calculations

In the designed systems heat is exchanged between the solid walls of the fuel processors and the fluids flowing through them or in certain cases between the hot and the cold fluids. The physical model calculations are based on FEM but computational fluid

dynamics (CFD) is not included. However, to still partially address the problem of heat transfer from the walls to the fluids or vice versa a temperature difference is used. For fluid–wall interaction heat exchange it is assumed that the geometry of fuel processors (e.g. thickness of walls, channel size and their distribution etc.) is designed in such a way that after the heat exchange is completed the temperature difference is 5 K. If a process or a reaction within the fuel processor is exothermic the exiting stream temperature (calculated in zero-dimensional model) is 5 K higher than the average volume temperature of the fuel processor (calculated in physical model). In case of endothermic process or reaction the exiting stream temperature is 5 K lower than the average volume temperature of the fuel processor.

Without CFD analysis the exact temperature distribution of the fluid–fluid interaction heat exchange is also unknown. Accordingly, an approximation is used where the temperature of all incoming and outgoing streams obtained from a zero-dimensional model is averaged to obtain the average volume temperature of the fuel processor. The fuel processor is positioned within the physical model on location where the temperature profile matches the average temperature obtained from the zero-dimensional model. This way a quasi-adiabatic state is achieved for the fluid–fluid interaction heat exchange because the external heat flow coming from hotter fuel processors is equilibrated with fuel processor heat losses.

3.3. Mass and energy balances

Mass and energy balances of the modelled systems are calculated using zero-dimensional models in Aspen Plus® software, version 7.2, released on 6-Jul-2010. In the modelled systems polar (water, methanol), non-electrolyte substances at a pressure of less than 10 bar are present, therefore, the non-random two-liquid – Redlich–Kwong (NRTL – RK) property method is selected to compute the thermodynamic properties. The calculations in Aspen Plus® are run based on the flowcharts presented in Section 2. The model of MSR (explained in Subsection 3.3.2) is the same in all cases and is dependent on temperature and incoming methanol flow. The model of PEMFC stack (explained in Subsection 3.3.1) is also the same in all cases but different polarisation curves and excess hydrogen ratios λ_{H_2} are used in calculations to reflect different types of PEMFC stacks. The model of PROX reactor (explained in Subsection 3.3.3) is used only in the case of LT PEMFC stack.

3.3.1. Fuel cell stack

A model of PEMFC stack was downloaded From Aspen Plus support site. It is based on User-2 model unit where a user subroutine is written in FORTRAN programing language. The programing code was modified in such a way that the rate of power production in the PEMFC depends on the incoming hydrogen flow. Based on accessible polarisation curves from commercial suppliers [10,43] (see also Fig. 6) the data for power density polynomial was calculated. Converting the molar flow of reacted hydrogen $\dot{n}_{H_2}$ into generated current density j is easily done via Faraday's law of electrolysis:

$$\dot{n}_{H_2} = \frac{j \cdot A}{2 \cdot F}, \tag{4}$$

where A is the active surface area of the PEMFC (identical for all three systems), 2 represents the number of charge carriers and F Faraday constant. Based on the power density curves and the active surface area $A = 25\ cm^2$, the number of cells in the system is determined. To achieve nominal power of 25 W four PEMFCs are needed in all three cases. The heat produced by the PEMFC stack is calculated as a difference between available energy and the power produced by the stack. The available energy is calculated as a difference in enthalpy of incoming and outgoing streams.

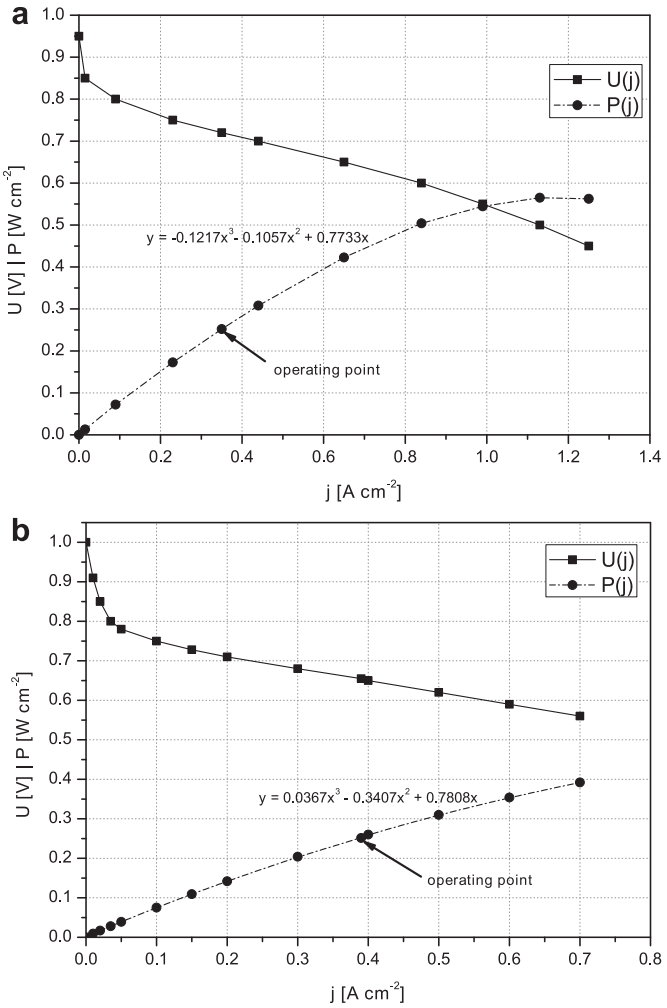

Fig. 6. Assumed power density curves used in simulations of PEMFCs operating on reformate gas are based on commercially available data: (a) LT PEMFC data based on GORE® PRIMEA® [43], (b) HT PEMFC data based on Celtec® P1100W [10].

In the PEMFC stack hydrogen does not react completely, some of it also leaves the system unutilised. In other words, the hydrogen is fed into the system with over stoichiometric ratio which is inversely proportional to hydrogen utilisation. In the models λ_{H_2} is equal to the specifications of suppliers, which is 1.2 for LT PEMFC and 1.4 for cHT PEMFC. Since no true data are available yet for nHT PEMFC the polarisation curve of cHT PEMFC is used instead. However, it is assumed that at such high temperatures problems with adsorption of CO will be even smaller (as shown in case of SAFC), hence, lower excess hydrogen ratio $\lambda_{H_2} = 1.2$ is adopted for the nHT PEMFC. All the systems are air cooled, therefore, to provide sufficient flow of cooling air the excess air ratio λ_{AIR} is greater as the one specified by suppliers, which is 2 for LT PEMFC and 5 for cHT PEMFC. For nHT PEMFC it is assumed that higher temperatures and the absence of phosphoric acid will indeed speed up the kinetics of ORR, hence, also lower excess air ratio than 5 can be used.

3.3.2. Methanol steam reformer

To properly describe the methanol conversion as a function of temperature the kinetic model proposed in Ref. [44] is used. The

same kinetic model was also used in other studies [16,45]. The values used for the model of the MSR are presented in Table 1.

The kinetic model presumes that in the MSR three reactions proceed simultaneously: methanol steam reforming (Eq. (5)), direct decomposition of methanol (Eq. (6)), and water-gas shift reaction (Eq. (7)):

$$CH_3OH + H_2O \leftrightarrow CO_2 + 3H_2, \tag{5}$$

$$CH_3OH \leftrightarrow CO + 2H_2, \tag{6}$$

$$CO + H_2O \leftrightarrow CO_2 + H_2. \tag{7}$$

The rate of reaction r depends on the rate limiting step in its set of elementary reaction steps. The overall process in the MSR is a combination of all three reaction sets; therefore, it is given in the form of the following equations:

$$r_R = \frac{k_R \cdot K^*_{CH_3O^{(1)}} \cdot \left(\frac{p_{CH_3OH}}{p^{1/2}_{H_2}}\right) \cdot \left(1 - \frac{p^3_{H_2} \cdot p_{CO_2}}{K_R \cdot p_{CH_3OH} \cdot p_{H_2O}}\right) \cdot C^T_{S_1} \cdot C^T_{S_{1a}} \cdot S_C \cdot \rho_b}{\left(1 + K^*_{CH_3O^{(1)}} \cdot \left(\frac{p_{CH_3OH}}{p^{1/2}_{H_2}}\right) + K^*_{HCOO^{(1)}} \cdot p_{CO_2} \cdot p^{1/2}_{H_2} + K^*_{OH^{(1)}} \cdot \left(\frac{p_{H_2O}}{p^{1/2}_{H_2}}\right)\right) + \left(1 + K^{1/2}_{H^{(1a)}} \cdot p^{1/2}_{H_2}\right)}, \tag{8}$$

$$r_D = \frac{k_D \cdot K^*_{CH_3O^{(2)}} \cdot \left(\frac{p_{CH_3OH}}{p^{1/2}_{H_2}}\right) \cdot \left(1 - \frac{p^2_{H_2} \cdot p_{CO}}{K_D \cdot p_{CH_3OH}}\right) \cdot C^T_{S_2} \cdot C^T_{S_{2a}} \cdot S_C \cdot \rho_b}{\left(1 + K^*_{CH_3O^{(2)}} \cdot \left(\frac{p_{CH_3OH}}{p^{1/2}_{H_2}}\right) + K^*_{OH^{(2)}} \cdot \left(\frac{p_{H_2O}}{p^{1/2}_{H_2}}\right)\right) + \left(1 + K^{1/2}_{H^{(2a)}} \cdot p^{1/2}_{H_2}\right)}, \tag{9}$$

$$r_W = \frac{k_W \cdot K^*_{OH^{(1)}} \cdot \left(\frac{p_{CO} \cdot p_{H_2O}}{p^{1/2}_{H_2}}\right) \cdot \left(1 - \frac{p_{H_2} \cdot p_{CO_2}}{K_W \cdot p_{CO} \cdot p_{H_2O}}\right) \cdot C^{T^2}_{S_1} \cdot S_C \cdot \rho_b}{\left(1 + K^*_{CH_3O^{(1)}} \cdot \left(\frac{p_{CH_3OH}}{p^{1/2}_{H_2}}\right) + K^*_{HCOO^{(1)}} \cdot p_{CO_2} \cdot p^{1/2}_{H_2} + K^*_{OH^{(1)}} \cdot \left(\frac{p_{H_2O}}{p^{1/2}_{H_2}}\right)\right)^2}. \tag{10}$$

Eqs. (8)–(10) are used in Aspen Plus process modelling software where a plug flow reactor (RPlug) model unit is used to simulate the MSR. R-Plug model unit assumes that perfect mixing occurs in the radial direction and that no mixing occurs in the axial direction. The reaction equations are integrated into the unit in the form of Langmuir–Hinshelwood–Hougen–Watson (LHHW) kinetic model.

The methanol conversion is also a function of methanol flow, catalyst loading and the MSR size. In Aspen plus only modelling of tubular reactors is possible. However, the conceived integrated systems are constructed from plate-type elements. Therefore, to get an estimate of the MSR dimensions for the physical model the tubular reactor volume used in the zero-dimensional model is converted into cuboid reactor volume. This is accomplished by exactly matching the cross-section surface area of the plate-type reactor to the cross-section surface area of the tubular reactor, while keeping the length of both reactors identical. Also, the plate-type MSR is split in two reactors where each is mounted on one side of the catalytic combustor (as shown in Section 2). The characteristics of the catalyst and the MSR used in zero-dimensional model

Table 1
Kinetic parameters for MSR modelling.

Parameter	Value	Unit
k_R	$7.4 \cdot 10^{14} \cdot \exp\left(-\frac{102.800}{R \cdot T}\right)$	$m^2\ mol^{-1}\ s^{-1}$
K_D	$3.8 \cdot 10^{20} \cdot \exp\left(-\frac{170.000}{R \cdot T}\right)$	$m^2\ mol^{-1}\ s^{-1}$
k_W	$5.9 \cdot 10^{14} \cdot \exp\left(-\frac{87.600}{R \cdot T}\right)$	$m^2\ mol^{-1}\ s^{-1}$
K_R	$10^{(1.4142 \cdot 10^{-13} \cdot T^5 - 4.2864 \cdot 10^{-10} \cdot T^4 + 5.3993 \cdot 10^{-7} \cdot T^3 - 3.6385 \cdot 10^{-4} \cdot T^2 + 1.4096 \cdot 10^{-1} \cdot T - 20.258)}$	bar^2
K_D	$10^{(2.9463 \cdot 10^{-13} \cdot T^5 - 8.8919 \cdot 10^{-10} \cdot T^4 + 11.1130 \cdot 10^{-6} \cdot T^3 - 7.4160 \cdot 10^{-4} \cdot T^2 + 2.7969 \cdot 10^{-1} \cdot T - 44.944)}$	bar^2
K_W	$10^{(-1.4936 \cdot 10^{-13} \cdot T^5 + 4.5026 \cdot 10^{-10} \cdot T^4 - 5.6216 \cdot 10^{-7} \cdot T^3 + 3.7206 \cdot 10^{-4} \cdot T^2 - 1.3726 \cdot 10^{-1} \cdot T + 24.537)}$	/
$K^*_{CH_3O^{(1)}}$	$\exp\left(\frac{-41.8}{R} - \frac{-20.000}{R \cdot T}\right)$	$bar^{-0.5}$
$K^*_{CH_3O^{(2)}}$	$\exp\left(\frac{30}{R} - \frac{-20.000}{R \cdot T}\right)$	$bar^{-0.5}$
$K^*_{HCOO^{(1)}}$	$\exp\left(\frac{179.2}{R} - \frac{100.000}{R \cdot T}\right)$	$bar^{-1.5}$
$K^*_{OH^{(1)}}$	$\exp\left(\frac{-44.5}{R} - \frac{-20.000}{R \cdot T}\right)$	$bar^{-0.5}$
$K^*_{OH^{(2)}}$	$\exp\left(\frac{30}{R} - \frac{-20.000}{R \cdot T}\right)$	$bar^{-0.5}$
$K_{H^{(1a)}}$	$\exp\left(\frac{-100.8}{R} - \frac{-50.000}{R \cdot T}\right)$	bar^{-1}
$K_{H^{(2a)}}$	$\exp\left(\frac{-46.2}{R} - \frac{-50.000}{R \cdot T}\right)$	bar^{-1}
$C^T_{S_1}$	$7.5 \cdot 10^{-6}$	$mol\ m^{-2}$
$C^T_{S_{1a}}$	$1.5 \cdot 10^{-5}$	$mol\ m^{-2}$
$C^T_{S_2}$	$7.5 \cdot 10^{-6}$	$mol\ m^{-2}$
$C^T_{S_{2a}}$	$1.5 \cdot 10^{-5}$	$mol\ m^{-2}$

Table 2
MSR and catalyst properties used in calculations.

Parameter	Value	Unit
Catalyst bulk density, ρ_b	1300	kg m^{-3}
Catalyst specific surface area, S_C	102,000	m^2 kg^{-1}
Catalyst bed void fraction	0.38	/
Length of reaction chamber	45	mm
Diameter of tubular reaction chamber	16.9	mm
Height of cuboid reaction chamber	3	mm
Width of cuboid reaction chamber	45	mm

are presented in Table 2 together with estimated dimensions of the MSR for the physical model.

3.3.3. PROX reactor

An ideal PROX catalyst should primarily meet the following key requirements: (i) high CO oxidation activity, (ii) low hydrogen oxidation activity, (iii) resistance to deactivation caused by CO_2 and H_2O, (iv) operation in the temperature region defined by the temperature levels of the MSR and the LT PEMFC. In general holds true for all PROX catalysts that lower temperatures allow higher CO selectivity SE_{CO} but lower CO conversion X_{CO}, while at higher temperatures conversion is enhanced but the selectivity drops [46–49]. The CO conversion also depends on the oxygen-to-CO molar ratio O_2/CO, which for a complete oxidation equals 0.5. Increasing the O_2/CO ratio to over stoichiometric also increases CO conversion and decreases CO selectivity of the PROX reaction because excess oxygen beyond complete CO oxidation is consumed by hydrogen and methanol oxidation reactions [49,50].

The catalyst selectivity towards CO oxidation in the reformate stream is defined as the ratio of oxygen molar flow consumed for CO oxidation over total oxygen molar flow consumed for oxidation of all combustible components:

$$SE_{CO} = \frac{0.5\cdot(\dot{n}_{CO,IN} - \dot{n}_{CO,OUT})}{\dot{n}_{O_2,IN} - \dot{n}_{O_2,OUT}} \tag{11}$$

In similar way selectivity towards hydrogen oxidation SE_{H_2} and methanol oxidation SE_{MeOH} can be written as:

$$SE_{H_2} = \frac{0.5\cdot(\dot{n}_{H_2,IN} - \dot{n}_{H_2,OUT})}{\dot{n}_{O_2,IN} - \dot{n}_{O_2,OUT}} \tag{12}$$

$$SE_{MeOH} = \frac{1.5\cdot(\dot{n}_{MeOH,IN} - \dot{n}_{MeOH,OUT})}{\dot{n}_{O_2,IN} - \dot{n}_{O_2,OUT}} \tag{13}$$

The conversion of CO during the PROX reaction is calculated as follows:

$$X_{CO} = \frac{\dot{n}_{CO,IN} - \dot{n}_{CO,OUT}}{\dot{n}_{CO,IN}} \tag{14}$$

Similarly, the conversion of hydrogen X_{H_2} and methanol X_{MeOH} are evaluated as:

$$X_{H_2} = \frac{\dot{n}_{H_2,IN} - \dot{n}_{H_2,OUT}}{\dot{n}_{H_2,IN}} \tag{15}$$

$$X_{MeOH} = \frac{\dot{n}_{MeOH,IN} - \dot{n}_{MeOH,OUT}}{\dot{n}_{MeOH,IN}} \tag{16}$$

The PROX reactor is modelled with RStoic model unit where, based on literature review, it is adopted that the PROX reaction proceeds at 155 °C, and excess air ratio of oxygen $\lambda_{O_2} = 2.5$. It is also assumed that all of the oxygen present in the reactor is consumed and that the selectivity for methanol, hydrogen and CO is 0.3, 0.3 and 0.4, respectively. On the basis of presumed operational conditions for the PROX reactor and the fact that the CO concentration in the reformate stream needs to be less than 10 ppm it is established that the conversion of CO, methanol and hydrogen is 99.8%, 47.7% and 0.5%, respectively.

3.4. Physical modelling of the systems

Physical modelling of the systems is performed using COMSOL Multiphysics® software, version 4.3, released on 17-May-2012. The same modelling approach based on FEM is used in all three systems. Within the systems only heat conduction is taken into account because all heat exchanges with fluids are modelled either as heat sources or heat sinks. The generic form of heat conduction equation used in COMSOL modelling is:

$$-\nabla\cdot(k\nabla T) = Q, \tag{17}$$

where k represents thermal conductivity which is considered to be isotropic and Q represents heat sources or sinks.

Natural convection is considered only in the case of heat transfer from the outer layer of insulation towards surroundings and in the case of LT PEMFC stack where the stack is directly exposed to surroundings. The generic form of heat transfer equation is:

$$-n\cdot(-k\nabla T) = h\cdot(T_{SURR} - T) \tag{18}$$

where n represents normal vector of outer surface and h heat transfer coefficient.

Due to heat conduction in the plate-type components temperature gradients appear. In vertical direction the temperature gradients mostly appear due to heat sources and heat sinks that represent different model units and on a smaller scale also due to heat losses. Far less pronounced are the gradients in lateral direction as they are caused only by heat losses to surroundings. Therefore, to properly estimate the temperature of individual plate-type component the volume average temperature is used. Different heat sources are used in the modelling of the systems. For PROX reactor and catalytic combustor a volume heat source is used and for each individual PEMFC a surface heat source is used. Similarly, the vaporiser, MSR and convective air cooling of bipolar plates are modelled as volume heat sinks. The properties of system components are presented in Table 3.

The symmetry of modelled systems allows to perform calculations on only 1/8 of the system and afterwards to extrapolate the results to the whole system. The FEM calculation process is stopped when the relative tolerance of successive calculated values is below 10^{-4}. Based on the value of total heat losses of the system grid independence is tested. First it is verified that during last iterations the calculated value is stable. Thereafter it has been established that the threefold refinement of mesh elements typically changes the calculated value for less than 0.2%.

4. Results and discussion

4.1. Water–methanol mixture

It is assumed that at the beginning water and methanol reside in two separated containers. Upon mixing, water and methanol form a non-ideal mixture with a mixing enthalpy of exothermic nature. This leads to a noticeable temperature rise of around 10 K for a mixture with water-to-methanol molar ratio 1.5.

A phase transition for the water–methanol mixture depends on its composition. A mixture with the molar ratio 1.5 has a phase

Table 3
Properties of materials considered for use in the integrated systems.

Fuel processor (system component)	Material	Thickness [mm]	Operating temperature [°C]	Heat conductivity [W m^{-1} K^{-1}]	Heat transfer coefficient [W m^{-2} K^{-1}]
End plate	Al-alloy	20	42	115	20
			79		/
			76		/
Bipolar plate	Graphite composite	4	70	43	20
			180		/
			255		/
Insulation	X-Aerogel	30 (outer)	20 (outer layer)	0.015	15
		varies (inner)	Up to 260 °C	0.024	/
Heat exchanger	LTCC wafer	3	100–255	5	/
PROX reactor		4	150		
MSR	Si wafer	5	255	70	/
Cat. combustor		4	255		

transition between 75 and 89 °C (see Fig. 7). This information is especially important when designing the vaporiser.

From an exergy point of view it is preferable to conduct the heat exchange at smaller temperature gradients (e.g. preheating, vaporising and superheating the water–methanol mixture in steps). However, care needs to be taken when designing such a system because otherwise partial vaporisation of water–methanol mixture might occur in certain system components. From an engineering point of view it is not desirable to have a two-phase flow running around the system because uncontrolled pulsations of pressures can occur while a fluid is expanding or contracting during the vaporisation or condensation. That is why the two-phase flow is avoided except in strictly defined fuel processors (vaporisers) where all of the water–methanol mixture is vaporized at once.

4.2. Sensitivity analysis of methanol steam reformer

First it should be pointed out that although the kinetic study of the MSR catalyst is very thorough it is based on an old catalyst. However, the results are still representative because they show dependence of methanol conversion in respect with molar flow and temperature. It is therefore safe to consider that using the same loading of modern catalyst either at lower temperature, higher methanol flow or smaller size of the MSR will still allow to achieve the same conversion rate of methanol. Most likely even higher conversion rate of methanol will be achieved. The Eq. (16) given for PROX reactor is in general form therefore it is also used to calculate methanol conversion rate in MSR.

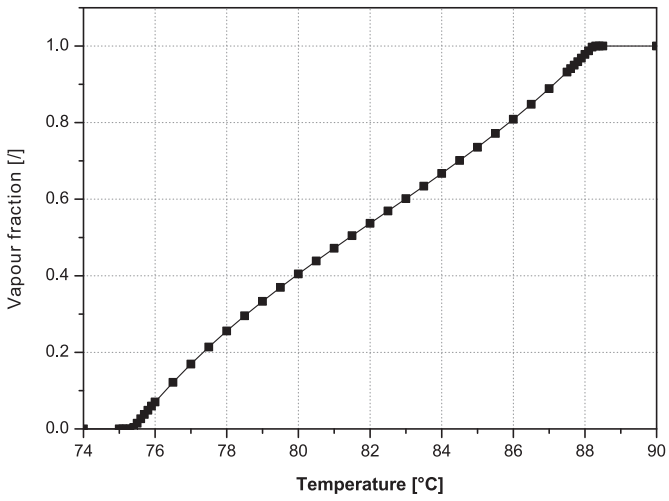

Fig. 7. Vapour fraction as a function of temperature for 1.5:1 water–methanol mixture.

In all three studies the same geometry of the MSR and the catalyst characteristics are used (see Table 2). To study the effect of operating temperature and incoming molar flow of water–methanol mixture on the methanol conversion rate, two sensitivity analyses are performed.

Fig. 8(a) shows that lowering the operating temperature of the MSR reduces the methanol conversion rate. On the other hand,

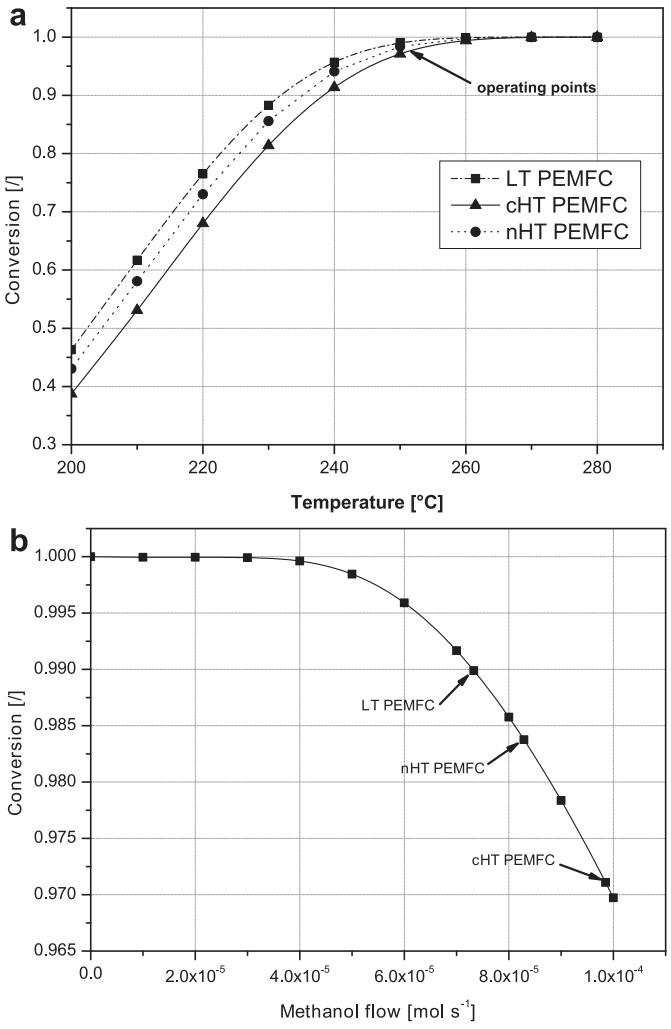

Fig. 8. Sensitivity analysis of MSR: (a) conversion of methanol as a function of temperature at fixed molar flow (25 We at 250 °C), (b) conversion of methanol as a function of molar flow at MSR operating temperature of 250 °C.

rising the temperature above 270 °C allows all the systems to practically achieve 100% conversion rate. The molar flow of water–methanol mixture is fixed during the analysis and it allows the PEMFC stack to produce 25 W of electric power when the operating temperature of the MSR is 250 °C.

Fig. 8(b) shows conversion rate as a function of methanol molar flow where the operating temperature of the MSR is fixed at 250 °C. The LT PEMFC stack uses the least methanol to produce 25 W of electricity. Presuming, that the beginning assumptions do hold true the nHT PEMFC stack will also use less methanol than the cHT PEMFC stack. This is the main reason why the methanol conversion is the best in case of the system with the LT PEMFC stack and the worst in case of the system with the cHT PEMFC stack. The exact figures of methanol conversion are given in Table 5.

Not only conversion of methanol is affected by the change of molar flow but also the composition of reformate stream. Table 4 shows that CO concentration is below 0.5% in all the systems. This however does not present any problems for operation of the cHT PEMFC or the nHT PEMFC stack but the permissible level of CO is significantly exceeded for the LT PEMFC stack. That is why the composition of the exit stream from the PROX reactor is given which shows that the level of CO is indeed reduced below 10 ppm. Due to hydrogen and methanol oxidation also around two percentage points of hydrogen are lost and the methanol concentration is reduced for about 50%.

4.3. Analysis of system with LT PEMFC stack

In terms of methanol consumption for the operation of PEMFC stack the system with LT PEMFC stack is the most efficient. This is due to the fact that Primea® fuel cells have higher power density than Celtec® 1100-W fuel cells. However, additional methanol is burned in the catalytic combustor to supply the required heat to the MSR. From the system point of view this significantly reduces its efficiency.

Based on the calculations from zero-dimensional model presented on Fig. 2(b) and the physical model shown on Fig. 9(b) the Sankey diagram on Fig. 9(a) is constructed. Out of 63.7 W of energy flow that is put into the system in the form of methanol 25 W is transformed into electric power and 18.5 W into heat flow in the LT PEMFC stack. To sustain the isothermal operation of the LT PEMFC stack at 70 °C only 5.1 W of heat flow is removed with cooling air. However, to achieve this, the system still requires high excess air ratio $\lambda_{AIR} = 9$ to be used. Because there is a small temperature difference between cooling air and the LT PEMFC stack high quantities of air do not remove much heat. Therefore, also natural convection is used to cool the LT PEMFC stack. If the system would not be allowed to cool by natural convection even larger amounts of cooling air would be needed. On one hand, natural convection greatly increases the heat losses of the system but on the other hand having vast amounts of air at 65 °C is of no practical use to the system because all the processes take place at higher temperatures. Blowing more air into the system also means more power consumption for the blower and introducing air with low temperature into combustor means that more fuel is used to raise the temperature of flue gases to the desired level. Moreover, even in this particular case a bypass is used to reduce the amount of air into the catalytic combustor and thus saving some methanol. Out of 19.6 W of total heat losses approximately 16.1 W represent losses due to cooling by natural convection and around 3.6 W are lost through the insulated part of the system. Although, the temperature of exiting flue gases is relatively low at 85 °C there are still 7.2 W of energy flow available for the external process and 11.9 W needs to be rejected to the surroundings.

Fig. 9(b) confirms that the initial assumption of isothermal operation of the fuel processors is valid. The catalytic combustor and the MSR operate at an average temperature of 255 °C and the difference between the hottest part of the combustor and the coldest part of the MSR is negligible. From zero-dimensional model the operational temperature of the water–methanol mixture superheater is determined to be 223 °C. The deviation in physical model is less than 0.5 K. To sustain the desired temperature a 2.5 mm thermal insulation layer is needed between the MSR and the superheater. A 3.5 mm thick insulation layer is required to sustain the PROX reactor operating at a volume average temperature of 150 °C. The PROX reactor is separated from the vaporiser

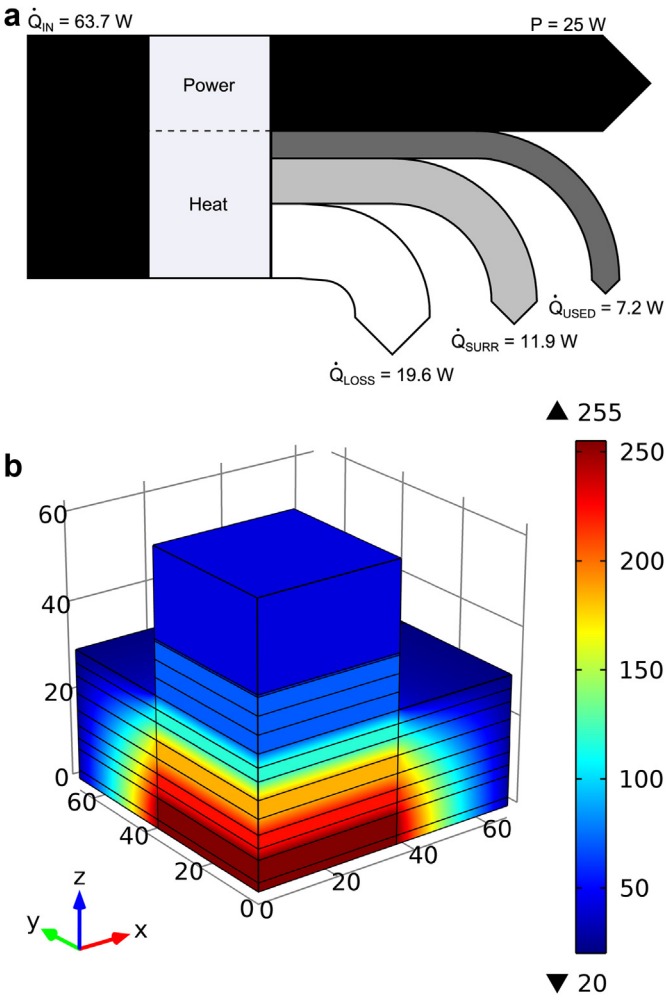

Fig. 9. Integrated system with LT PEMFC stack: (a) Sankey diagram of energy flows, (b) temperature profile of the designed system.

Table 4
Molar composition of the reformate stream for the compared systems.

System	nHT PEMFC	cHT PEMFC	LT PEMFC	LT PEMFC (after PROX)
H_2	0.6559	0.6510	0.6584	0.6377
H_2O	0.1203	0.1239	0.1183	0.1223
CO	0.0046	0.0049	0.0044	0[a]
CO_2	0.2155	0.2137	0.2165	0.2161
O_2	0	0	0	0
N_2	0	0	0	0.0226
CH_3OH	0.0037	0.0065	0.0023	0.0012

[a] Calculated value is less than 9 ppm.

with a 4 mm thick insulation. The calculated average volume temperature of the vaporiser is 118 °C. If the vaporiser would be in direct thermal contact with the PROX reactor its temperature would equilibrate with the operating temperature of the PROX reactor. Meaning, the temperature of the vaporiser would be too high and the reformate stream would not cool down to the appropriate temperature before entering the LT PEMFC stack. A 3 mm thick insulation is required to provide the desired temperature difference between the vaporiser and the LT PEMFC stack. Even though the LT PEMFC stack is cooled by the cathode air as well as by natural convection the difference between the hottest and the coldest side is only 0.2 K and hence considered negligible. This shows that thermal conductivity of bipolar plates is sufficiently high to allow the LT PEMFC stack to operate at practically isothermal conditions. A thin 0.5 mm thick insulating layer is needed between the LT PEMFC stack and the aluminium alloy plate. If the insulating layer is thicker the stack begins to overheat because there is not enough heat transferred to the surroundings via the natural convection from the end plate.

4.4. Analysis of system with cHT PEMFC stack

Since the cHT PEMFC stack uses the highest λ_{H_2} among the modelled PEMFC stacks the methanol consumption is also the highest. Because cHT PEMFC is not allowed to heat up above 180 °C, this would eventually lead to irreversible damage to the PEMFC, the excess heat that could otherwise be used for the MSR is on too low temperature level. On the other hand, higher λ_{H_2} allows utilising the unreacted hydrogen in a reasonably efficient way because the additional heat needed for the MSR is produced when anode off-gas is burned in the catalytic combustor.

The Sankey diagram on Fig. 10(a) is constructed based on zero-dimensional model presented on Fig. 3(b) and the physical model shown on Fig. 10(b). As seen from Fig. 10(a) energy flow into the system is 69.7 W. In the cHT PEMFC stack 25 W is transformed into electric power and 24.3 W into heat flow. To sustain the isothermal operation of the cHT PEMFC stack 16.5 W of heat flow needs to be removed with cooling air. Cooling is much more efficient than in the case of LT PEMFC stack because the temperature difference between the cooling air and the cHT PMEFC stack is considerably larger, hence lower λ_{AIR} can be used. Also, natural convection must be prevented because of the high operating temperatures and the system must be entirely insulated. Here, high temperature flue gases at 254 °C can efficiently be put to use, hence 30.2 W of heat flow is available for use in the external process. Because the system is fully insulated the smallest heat losses among all the systems are achieved. The heat losses through the insulation accumulate to 3.4 W and there are 11.1 W that still need to be rejected to the surroundings.

From Fig. 10(b) it is seen that the fuel processors achieve practically isothermal conditions of operation. The catalytic combustor and the MSR operate at an average temperature of 256 °C. Because of the high thermal conductivity of silica wafer the difference between the hottest part of the combustor and the coldest part of the MSR is negligible. The calculated volume average temperature of the superheater is 216 °C which is approximately in the middle between the operating temperatures of the MSR and the cHT PEMFC stack. On the hotter side a 1.8 mm thermal insulation layer is needed and on the colder side a 1.6 mm thick insulation layer is needed to sustain the operating temperature. The cHT PEMFC stack operates at a volume average temperature of 181 °C where the difference between the hottest and the coldest part is less than 0.5 K. A 1.4 mm thick insulation is required to provide the desired temperature difference between the cHT PEMFC stack and the vaporiser which operates at 100 °C. To sustain the operating

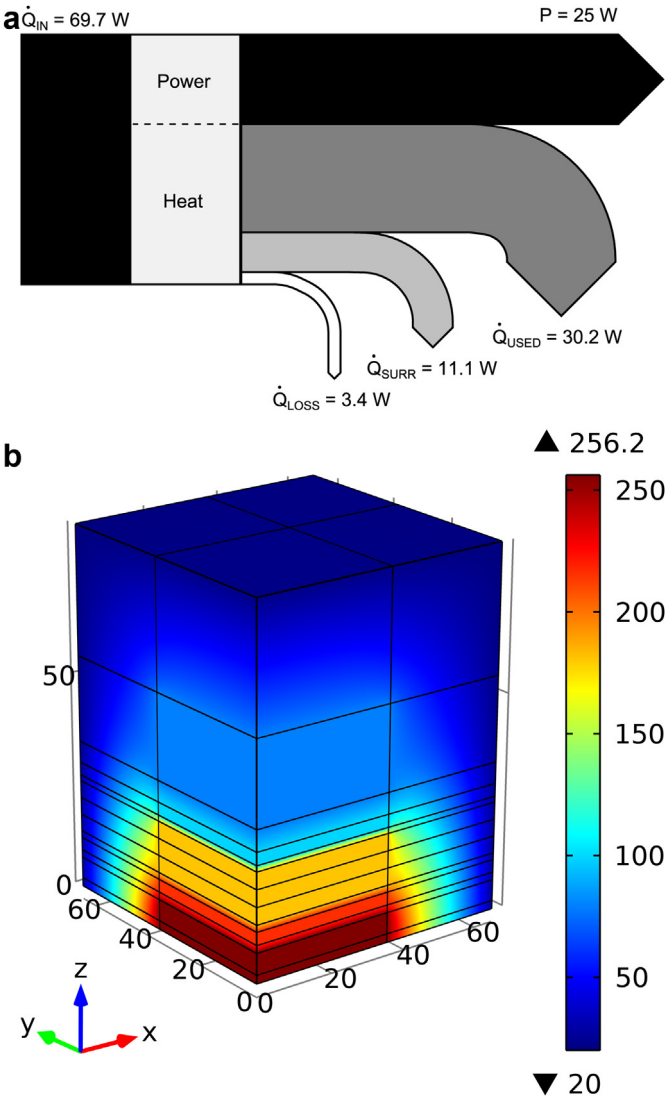

Fig. 10. Integrated system with cHT PEMFC stack: (a) Sankey diagram of energy flows, (b) temperature profile of the designed system.

temperature the vaporiser also requires a 5 mm thick insulation against the aluminium alloy end plate.

4.5. Analysis of system with nHT PEMFC stack

The least methanol is used in the system with nHT PEMFC stack. This is directly reflected in the efficiency of the system which is the highest among all systems. The Sankey diagram on Fig. 11(a) is constructed based on zero-dimensional model presented on Fig. 4(b) and the physical model shown on Fig. 11(b). As seen on Fig. 11(a) 59.3 W of energy flow is put into the system in the form of methanol. In the nHT PEMFC stack 25 W are transformed into electric power and 24.4 W into heat flow. To sustain the isothermal operation of the cHT PEMFC stack 15.6 W of heat flow needs to be removed with cooling air. Cooling is efficient because the temperature difference between the cooling air and the nHT PMEFC stack is very large hence the lowest λ_{AIR} can be used. The system is fully insulated and operates at the highest temperatures among all compared systems. This is the reason why the heat losses through the insulation are the highest and accumulate to 3.8 W. The exiting temperature of flue gases is 260 °C and can efficiently be put to use,

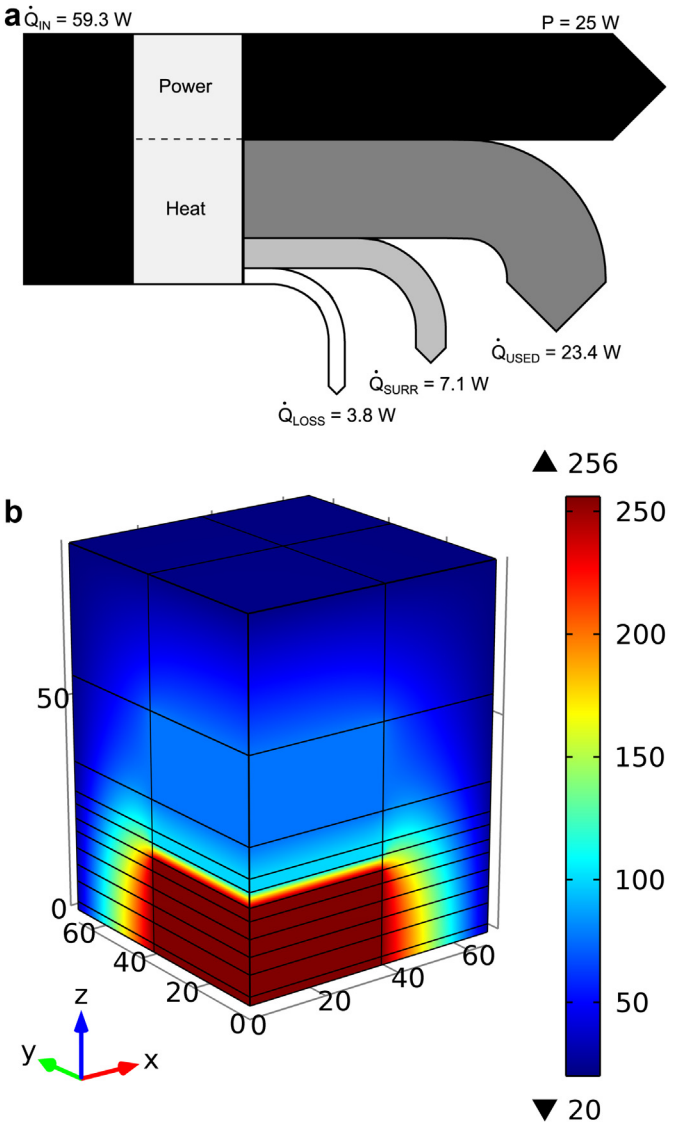

Fig. 11. Integrated system with nHT PEMFC stack: (a) Sankey diagram of energy flows, (b) temperature profile of the designed system.

hence 23.4 W of heat flow is available for use in the external process. There are 7.1 W that still need to be rejected to the surroundings.

The devised system with the HT PEMFC stack resembles the system with the cHT PEMFC as both systems are fully insulated. The main difference is that here almost entire system operates at a temperature of 256 °C. Because the fuel processors are relatively thin the heat transfer between them is mainly attributed to the heat conductivity of materials. The calculations show that in a steady state only a slight temperature difference of 1 K is created between the hottest part of the combustor and the coldest part of the superheater. The vaporiser which operates at 100 °C is separated from the hot part of the system with 3.5 mm thermal insulation layer and on the other side a 7 mm thick insulation layer is needed to separate it from the aluminium alloy end plate. The temperature profile of the integrated system is presented on Fig. 11(b).

4.6. Discussion

The performance characteristics of integrated systems are summarized in Table 5 and further discussed hereinafter. Since all input and output streams are at ambient conditions the calculated gross electric efficiency η_{EL} and gross cogeneration efficiency η_{COG} are based on higher heating value (HHV) and are defined as follows:

$$\eta_{EL} = \frac{P}{\dot{Q}_{IN}} \tag{19}$$

$$\eta_{COG} = \frac{P + \dot{Q}_{USED}}{\dot{Q}_{IN}} \tag{20}$$

The external process is not included in calculations of heat transfer among the system fuel processors because it is not a part of the integrated system. However, it has been foreseen that this process is still a part of the overall (cogeneration) system. Therefore, η_{EL} gives the efficiency of integrated PEMFC stack and MSR system while cogeneration system efficiency η_{COG} gives the system efficiency after the exhaust flue gases are cooled down to 40 °C.

The highest methanol consumption and consequently the lowest electric efficiency are achieved in the system with cHT PEMFC. This is due to the fact that the system uses the highest λ_{H_2} among all. Even though the LT PEMFC stack uses the smallest amount of methanol the electric efficiency of the system is still lower than in the case of the system with nHT PEMFC stack because additional methanol is required to provide heat for the MSR. Therefore, the best gross electric efficiency is achieved by the system with nHT PEMFC stack.

As a result of low operating temperature considerably lower combined system efficiency is attained in case of the system with LT PEMFC stack. Due to higher operating temperature both systems with HT PEMFC stacks are able to use the heat of flue gases more efficiently and hence achieve higher system efficiencies.

Operating temperature also affects the excess air ratio. The effect is clearly seen in the case of LT PEMFC stack which requires substantially more air to sustain the required temperature than both HT PEMFC stacks. The ratio would be even higher if the LT PEMFC stack would not be allowed to cool by natural convection. Even though this way considerable part of energy flow is lost it is not on very high temperature level and therefore of no practical use to the system because all the processes take place at higher

Table 5
Comparison of the integrated systems.

Integrated system	Stack temp.	Gross electric efficiency	Gross cogeneration efficiency	Methanol consumption	Methanol conversion	Excess air	Heat losses
LT PEMFC	70 °C	39.2%	50.5%	$7.34 \cdot 10^{-5}$ mol s^{-1} [a] $1.64 \cdot 10^{-5}$ mol s^{-1} [b]	99.0%	9.0	16.1 W [c] 3.6 W [d]
cHT PEMFC	180 °C	35.9%	79.2%	$9.8 \cdot 10^{-5}$ mol s^{-1}	97.1%	7.4	3.4 W
nHT PEMFC	255 °C	42.2%	81.6%	$8.3 \cdot 10^{-5}$ mol s^{-1}	98.3%	4.7	3.8 W

[a] Used in the MSR.
[b] Used in the catalytic combustor.
[c] Uninsulated part of the system (natural convection).
[d] Insulated part of the system.

temperatures. Due to higher temperature difference between the cooling air and both types of HT PMEFC stacks cooling is much more efficient in those systems, hence lower λ_{AIR} is used. This means that the blower will use less power which will further help to enhance net system efficiencies. High excess air can also cause problems in reaching the operating temperature of the catalytic combustor. A viable solution is to bypass part of the air past the combustor as in case of LT PEMFC stack and cHT PEMFC stack; however this will add certain complexity to both of the systems.

Heat losses are the lowest in case of the cHT PEMFC stack because the system is fully insulated. Because of higher operating temperature, higher heat losses occur in case of the system with nHT PEMFC stack. However, with proper distribution of heat sources and heat sinks within the system and adequate insulation within and around the system the heat losses are only 12% higher than in the case of the system with cHT PEMFC stack. Naturally, heat losses are the highest in the case of system with LT PEMFC stack because the system is left to cool by natural convection.

The key component for all modelled systems is the thermal insulation with extremely good insulating properties and resistance to compression forces. It is clearly shown that it enables the system to achieve desired temperatures of fuel processors using relatively thin thermal insulation layers; hence, it helps to keep the systems in a small and compact form. It also acts as an electric and most importantly as thermal insulator of aluminium alloy end plates. This is especially important in the case of HT PEMFC stack systems because the end plates are kept at a relatively low temperature compared to the operating temperature of the stacks. Aluminium is a very good thermal conductor and would contribute to substantial heat losses if the end plates were left to reach high temperatures especially because they are relatively thick and consequently have a large surface area. Most of aluminium alloys also tend to soften at temperatures above 200 °C. With this the structural stability of the system can be compromised and can even cause hydrogen leakage because the required stress on the gaskets is lost. Therefore, lower temperature of end plates also allows the use of more conventional, low-cost aluminium alloys as opposed to special, high-cost aluminium alloys that still maintain their structural stability at high temperatures.

5. Conclusions

This article demonstrates the concept of compact and highly integrated system with the MSR and the PEMFC stack. Here, the current state of R&D and the commercial market related to the technology of MSR–PEMFC-stack integrated systems is reviewed and examined. Issues that need to be resolved prior to constructing such systems are pointed out and also certain solutions or guidelines for solving them are discussed. Despite their small size such systems are still quite complex; therefore certain approximations are adopted in calculations. However, the modelling approach used serves as the quantitative basis for assessment and comparison of the proposed integrated systems.

The best performance among the modelled systems shows the system with nHT PEMFC stack. There are several reasons why this system promises to be the most effective. First, no additional methanol is needed to supply heat to the MSR. Second, high operating temperature and the materials from which the nHT PMEFC will be composed of will presumably allow it to operate on reformate gas where $\lambda_{H_2} = 1.2$ and thus be more economical in fuel consumption. Third, the lowest excess air ratio is used which allows the catalytic combustor to attain the operating temperature without the use of air bypass. The indirect effect will also be smaller power consumption by the blower. Fourth, high operating temperature of the nHT PEMFC stack enables to efficiently recuperate heat produced within the system and efficiently use the heat of flue gases in the external process.

However it is true, that currently no such commercial PEMFC exists. The technology and materials to build such an assembly are already at hand however they need to be carefully selected and correctly applied. That is why further research will be intensively focused on the development of components for the nHT PEMFC stack.

As mentioned in the introduction another path of research is opening for the integrated MSR–PEMFC-stack systems. A newly developed catalyst could enable direct thermal coupling of the LT MSR and the cHT PEMFC stack. This would create conditions similar to those in the system with nHT PEMFC stack and the efficiency of the system could be raised. Further studies will also be devoted to thermal coupling of such system.

Acknowledgements

Part of this work was carried out within the Centre of Excellence for Low-Carbon Technologies (CO NOT), Hajdrihova 19, 1000 Ljubljana, Slovenia.

The authors would also like to thank dr. Andrej Pohar, Institute of Chemistry Slovenia, Laboratory of Catalysis and Chemical Reaction Engineering, Hajdrihova 19, 1000 Ljubljana, Slovenia; for constructive discussions and guidance in the design and simulations of the integrated systems.

Nomenclature

Acronyms and abbreviations

BoP	balance-of-plant
CFD	computational fluid dynamics
cHT	conventional high-temperature
DMFC	direct methanol fuel cell
FEM	finite element method
HHV	higher heating value
HT	high-temperature
LHHW	Langmuir–Hinshelwood–Hougen–Watson
LT	low-temperature
MSR	methanol steam reformer
nHT	novel high-temperature
NRTL – RK	non-random two-liquid – Redlich–Kwong
ORR	oxygen reduction reaction
PBI	polybenzimidazole
PEMFC	proton exchange membrane fuel cell
PROX	preferential oxidation
SAFC	solid acid fuel cell
SATP	standard ambient temperature and pressure
TEG	thermo electric generator
WGS	water-gas shift

Symbols

A	active surface area of PEMFC, cm^2
$C^T_{S_i}$	total surface concentration of site i, mol m^{-2}
d	thickness of insulating layer, m
F	Faraday constant, A s mol^{-1}
h	heat transfer coefficient, W m^{-2} K^{-1}
j	current density, A cm^{-2}
k	thermal conductivity, W m^{-1} K^{-1}
k_i	rate constant for reaction i; m^2 s^{-1} mol^{-1}
K_i	equilibrium constant of reaction i; units are specific to the form of rate expression
$\dot{n}$	molar flow, mol s^{-1}
P	gross power produced by the system, W

p_{AMB}	ambient pressure, bar
p_i	partial pressure of species *i*, bar
T	temperature, K or °C
$\dot{Q}$	heat flow, W
R	universal gas constant, J mol^{-1} K^{-1}
r_i	rate of reaction *i*, mol s^{-1} m^{-3}
S_C	catalyst specific surface area, m^2 kg^{-1}
S_i	active site *i* in reaction mechanism
SE_i	selectivity towards species *i*
S/C	steam-to-carbon ratio
X_i	conversion rate of species *i*

Greek symbols

η	efficiency of the system
λ	above stoichiometric ratio
ρ_b	catalyst bulk density, kg m^{-3}

Subscripts

1	active site 1 when on variable *S*
1a	active site 1a when on variable *S*
2	active site 2 when on variable *S*
2a	active site 2a when on variable *S*
a, b	indicates an alternate route to a surface intermediate
AIR	air
CO	carbon monoxide
COG	cogeneration
COMB	referred to heat produced by the catalytic combustor
D	methanol decomposition; Eq. (6)
EL	electric
H_2	hydrogen
IN	incoming quantity
INSU	insulation
LOSS	referred to heat losses
MeOH	methanol
O_2	oxygen
OUT	outgoing quantity
PROCESS	referred to operating conditions of the process
PROFILE	referred to temperature profile of the system
PROX	referred to heat produced by the PROX reactor
R	methanol steam reforming process; Eq. (5)
STACK	referred to heat produced by the PEMFC stack
SURR	surroundings
USED	referred to heat used in external process
VAPO	referred to heat consumed by the vaporizer
W	WGS process; Eq. (7)

Superscripts

(*i*)	species adsorbed on active site *i* where *i* is 1, 1a, 2 or 2a
T	indicating total concentration of active sites

References

[1] A. Mishra, R. Prasad, Bull. Chem. React. Eng. Catal. 6 (2011) 1–14.
[2] J.-H. Wee, K.-Y. Lee, J. Power Sources 157 (2006) 128–135.
[3] C.-Y. Chen, W.-H. Lai, W.-M. Yan, C.-C. Chen, S.-W. Hsu, J. Power Sources 243 (2013) 138–146.
[4] L.-Y. Sung, B.-J. Hwang, K.-L. Hsueh, W.-N. Su, C.-C. Yang, J. Power Sources 242 (2013) 264–272.
[5] S. Choudhury, in: S. Basu (Ed.), Recent Trends in Fuel Cell Science and Technology, Springer, New York, 2007, pp. 188–216.
[6] Q. Li, R. He, J.O. Jensen, N.J. Bjerrum, Fuel Cells 4 (2004) 147–159.
[7] S.K. Das, A. Reis, K.J. Berry, J. Power Sources 193 (2009) 691–698.
[8] S.J. Andreasen, J.R. Vang, S.K. Kær, Int. J. Hydrogen Energy 36 (2011) 9815–9830.
[9] Advent, Advent TPS® HT MEA, http://www.advent-energy.com/prod_ht_pem.aspx (accessed 28.01.14).
[10] BASF, Celtec®; P1100W, http://www.fuel-cell.basf.com/cm/internet/Fuel_Cell/en_GB/, (accessed 28.1.2014).
[11] K.C. Neyerlin, A. Singh, D. Chu, J. Power Sources 176 (2008) 112–117.
[12] C. Korte, in: D. Stolten, B. Emonts (Eds.), Fuel Cell Science and Engineering, Wiley-VCH Verlag GmbH & Co. KGaA, Weinheim, Germany, 2012, pp. 335–359.
[13] M. Mamlouk, K. Scott, Int. J. Hydrogen Energy 35 (2010) 784–793.
[14] K.M.K. Yu, W. Tong, A. West, K. Cheung, S.C.E. Tsang, Y. Guo, T. Li, G. Smith, Nat. Commun. 3 (2012).
[15] W. Tong, K. Cheung, A. West, K.-M. Yu, S.C.E. Tsang, Phys. Chem. Chem. Phys. 15 (2013) 7240–7248.
[16] A.V. Pattekar, M.V. Kothare, J. Power Sources 147 (2005) 116–127.
[17] J.Y. Won, H.K. Jun, M.K. Jeon, S.I. Woo, Catal. Today 111 (2006) 158–163.
[18] Y. Men, G. Kolb, R. Zapf, D. Tiemann, M. Wichert, V. Hessel, H. Löwe, Int. J. Hydrogen Energy 33 (2008) 1374–1382.
[19] T. Kim, Int. J. Hydrogen Energy 34 (2009) 6790–6798.
[20] K.-F. Lo, S.-C. Wong, Int. J. Hydrogen Energy 36 (2011) 10719–10726.
[21] C. Pan, R. He, Q. Li, J.O. Jensen, N.J. Bjerrum, H.A. Hjulmand, A.B. Jensen, J. Power Sources 145 (2005) 392–398.
[22] J.D. Morse, R.S. Upadhye, R.T. Graff, C. Spadaccini, H.G. Park, E.K. Hart, J. Micromech. Microeng. 17 (2007) S237.
[23] A. Hindhede Jensen, L. Qingfeng, E. Christensen, N.J. Bjerrum, J. Electrochem. Soc. 161 (2014) F72.
[24] Q. Geletu, K. Ryuji, T. Atsushi, S. Takashi, S.T. Oyama, J. Electrochem. Soc. 161 (2014) F451.
[25] D.A. Boysen, T. Uda, C.R.I. Chisholm, S.M. Haile, Science 303 (2004) 68–70.
[26] T. Uda, S.M. Haile, Electrochem. Solid-State Lett. 8 (2005) A245–A246.
[27] C.R.I. Chisholm, D.A. Boysen, A.B. Papandrew, S. Zecevic, S. Cha, K.A. Sasaki, A. Varga, K.P. Giapis, S.M. Haile, Interface 18 (2009) 53–59.
[28] E. Romero-Pascual, J. Soler, Int. J. Hydrogen Energy 39 (2014) 4053–4059.
[29] W. Wu, C.-C. Pai, J. Power Sources 194 (2009) 920–930.
[30] H. Chang, H.C. Chiang, Y.H. Chen, Y.Y. Chang, S.H. Cheng, Chem. Eng. Sci. 74 (2012) 27–37.
[31] S. Authayanun, M. Mamlouk, K. Scott, A. Arpornwichanop, Appl. Energy 109 (2013) 192–201.
[32] R.S. Besser, Int. J. Hydrogen Energy 36 (2011) 276–283.
[33] K. Shah, R.S. Besser, J. Power Sources 166 (2007) 177–193.
[34] D. Wichmann, P. Engelhardt, R. Wruck, K. Lucka, H. Köhne, in: Fuel Cell Seminar and Exposition, Palm Springs, 2009.
[35] D. Wichmann, P. Engelhardt, R. Wruck, K. Lucka, H. Köhne, ECS Trans. 26 (2010) 505–515.
[36] G. Kolb, K.P. Schelhaas, M. Wichert, J. Burfeind, C. Heßke, G. Bandlamudi, Chem. Eng. Technol. 32 (2009) 1739–1747.
[37] S.J. Andreasen, S.K. Kær, Int. J. Hydrogen Energy 33 (2008) 4655–4664.
[38] T. Kurz, J. Keller, Fuel Cells 11 (2011) 518–525.
[39] X. Gao, S.J. Andreasen, M. Chen, S.K. Kær, Int. J. Hydrogen Energy 37 (2012) 8490–8498.
[40] D.T. Santa Rosa, D.G. Pinto, V.S. Silva, R.A. Silva, C.M. Rangel, Int. J. Hydrogen Energy 32 (2007) 4350–4357.
[41] M.A.B. Meador, E.J. Malow, R. Silva, S. Wright, D. Quade, S.L. Vivod, H. Guo, J. Guo, M. Cakmak, ACS Appl. Mater. Interfaces 4 (2012) 536–544.
[42] G.-B. Jung, H.-H. Chen, W.-M. Yan, J. Power Sources 247 (2014) 354–359.
[43] GORE, GORE®, PRIMEA® MEAs, http://www.gore.com/en_xx/products/electronic/fuelcells/series_56_mea_fuel_cells.html (accessed 28.01.14).
[44] B.A. Peppley, J.C. Amphlett, L.M. Kearns, R.F. Mann, Appl. Catal. A: Gen. 179 (1999) 31–49.
[45] J. Telotte, J. Kern, S. Palanki, Int. J. Chem. React. Eng. 6 (1) (2008).
[46] G. Avgouropoulos, T. Ioannides, C. Papadopoulou, J. Batista, S. Hocevar, H.K. Matralis, Catal. Today 75 (2002) 157–167.
[47] T. Komatsu, A. Tamura, J. Catal. 258 (2008) 306–314.
[48] X. Yu, H. Li, S.-T. Tu, J. Yan, Z. Wang, Int. J. Hydrogen Energy 36 (2011) 3778–3788.
[49] Q. Zhang, L. Shore, R.J. Farrauto, Int. J. Hydrogen Energy 37 (2012) 10874–10880.
[50] R.K. Ahluwalia, Q. Zhang, D.J. Chmielewski, K.C. Lauzze, M.A. Inbody, Catal. Today 99 (2005) 271–283.